An Electrodeless Technique for Full Scale Simulation of the Re-Entry Environment

Donald D. Hollister
Aeronutronic, A Division of the Philco Corporation

AN ELECTRODELESS TECHNIQUE FOR FULL SCALE SIMULATION OF THE RE-ENTRY ENVIRONMENT

Donald D. Hollister
Aeronutronic, A Division of the Philco Corporation
Newport Beach, California

Summary

A current need exists for improved methods in the ground testing of re-entry vehicles; it is believed that this need may soon become acute. Based on the arc-jet, the present generation of re-entry simulators is limited in exhaust enthalpy, physical size and purity of exhaust plasma. An electrodeless technique of plasma production at very high power levels has been developed, however, which removes many of these restrictions. In addition, the properties of a plasma generator based on the electrodeless discharge are such that the discharge can be maintained over a very wide range in applied power and gas density, and can be electronically controlled. It is thus possible that an entire entry trajectory can be reduced to data on punched cards which are fed into a computer that electronically controls the reproduction of the entry conditions for an arbitrary trajectory in an arbitrary atmosphere at the surface of a test model. A mathematical scaling law is presented which indicates that re-entry simulation based on the electrodeless technique can be extended to the full-scale case.

Introduction

The re-entry environment is typified by physical conditions of such extreme severity that the study of re-entry phenomena has itself become an important modern research specialty. The problems we face in the development of returnable space vehicles, both manned aerodynamic high L/D vehicles, and manned or unmanned ballistic re-entry bodies, are both numerous and profound. Other interesting problems are suggested by the prospect of extra-terrestrial landing missions. A landing after passage through an alien atmosphere, for example that of the planet Mars, will levy an entirely new generation of aerothermochemical entry questions on the terrestrial aerospace industries. Eventually, these questions, in exchange for progress, will demand answers.

Fortunately, for the present, with the current rapid progress in ablative materials' development, we are able to concentrate on one-way unmanned landers and experience no pressing demand for advanced entry studies, other than those now in progress. It seems quite clear, however, that the future will soon be upon us. Man will soon journey to the Moon and will eventually reach Mars. There is even now a great deal of interest in the thought of travel to one or more of the Jovian moons, the same degree of interest, it must be added, as was shown in the concept of a trip to the Moon in the late 1940's. Indeed, one must conclude that man finally has been committed to take the daring evolutionary step of space travel.

Each manned space mission has a common terminus, Earth. Each manned space mission must therefore end in an entry maneuver, and face the rigors of re-entry into the terrestrial atmosphere. Certain unmanned missions must also face re-entry; indeed, as the degree of technological sophistication of terrestrial satellites increases one naturally expects to observe a substantial increase in the number of

returnable, highly instrumented spacecraft. In a similar fashion, as Man's instrumented probes increasingly penetrate the depths of space the need for returnable inter-planetary spacecraft will appear. By the time an interplanetary mission requires a man on board, however, the need will have become acute.

The problem can be stated as follows: Present generation space vehicles are adequate for their present purposes, yet have stretched our technology to its limit.

A possible solution of the problem is the subject of this paper: Full scale ground testing of space vehicles. In this manner it is possible to measure that which cannot be computed (entry corridor limits in the Martian atmosphere as a function of absolute entry velocity for a particular vehicle, for example) in a fashion exactly analogous to the ground testing of aircraft, and for essentially the same purposes.

In the ensuing paragraphs a mechanism for accomplishing this will be described. What is known will be demonstrated, what must be learned will be stated. Since, however, the re-entry environment is to be simulated, it is advantageous at this point to digress to a very brief description of the pertinent phenomena in a re-entry situation.

As a space vehicle approaches a planet it first experiences a few inconsequential collisions with gas molecules at the upper limit of the planetary atmosphere. At such extreme altitudes the molecular mean free path λ is much greater than any characteristic vehicle dimension D, and there is no appreciable interaction between the particles incident at the vehicle's surface and those particles which were previously reflected from the surface. The energy transfer to the vehicle is entirely a surface effect and there is practically no viscous force on the vehicle due to atmospheric friction. This flight regime is characterized by the description, "free molecular flow" and is simply defined as that flow regime in which the Knudsen number K_n ($= \lambda / D$) is much greater than unity.

Atmospheric density increases with decreasing altitude. As the vehicle submerges deeper into the atmosphere the frequency of collisions between the particles reflected from the surface of the vehicle and those in the path of the vehicle increases. Relative to the vehicle, the particles in its path formerly approached with the vehicular velocity, collided with the vehicle, and were reflected. As the atmospheric density increases the reflected particles begin to collide with those incident, perturbing the velocity of the incident particle stream. With atmospheric penetration the interaction between incident and reflected particles becomes very pronounced, and a shock wave begins to appear a short distance from the vehicle, and across its path. By the time the shock wave is fully developed the mass flow between the shock and the vehicle surface is completely viscous, yielding what can best be described as a strong thermodynamic interaction between the vehicle and its environment. Ionizing collisions take place between incident and reflected particles, and between individual particles at the shock discontinuity. Viscous energy transfer, now enhanced by the effect of radiation from the shock and viscous layers and recombination, takes place at the vehicle surface at which an enormous amount of heat develops. At this stage any aerodynamic imperfection on the vehicular surface begins to burn away, or, if the vehicular surface is inadequate for the environment, the surface itself burns away in a process called ablation. The heat thus removed is partially evidenced, as is the heating of the vehicle itself, by a decrease in the velocity of the vehicle. Eventually this viscous force approaches in magnitude the gravitational force and a "terminal velocity" is reached. The kinetic and potential energies of the vehicle are thus considerably reduced by atmospheric friction, and are dissipated as ablation, and heat, and also by radiation. The eventual employment of the vehicle's

aerodynamic surfaces, retrorockets, or parachutes brings the vehicle to "soft landing" velocity, and the maneuver is completed.

The difficulties associated with the high heating rates developed during entry have largely been, and are being solved by controlled ablation. Aside from the creation of an unmistakable wake signature, the only essential drawback of the ablation cooling technique is the unfortunate fact that the mass content of the ablative skin of the vehicle is, during entry, a function of time, hence the useful life of such a vehicle is limited. In the case of extreme entry velocities ($\sim$ 50,000 ft/sec, for example) Roberts[1] estimates that up to 20 percent of the total vehicle mass would be lost by ablation during entry.

Another serious problem is communication. It is during the heavy ablation phase of the entry maneuver that communication from, and/or communication to the vehicle becomes extremely difficult, if not impossible. The ionized gas in the neighborhood of the vehicle, although electrically neutral (i.e., a plasma), usually has a sufficient density of free electrons to totally reflect incident radiofrequency energy.[2,3]

In itself, the several minutes of radio "blackout" concomitant with re-entry is of no profound significance at this time. In the future, however, a manned vehicle may plunge into our atmosphere a few degrees off course, subjecting the astronaut pilot to a sudden, and possibly incapacitating deceleration. The local plasma will then become an impenetrable communication barrier between space ship and earth, so that terrestrial control which could normally alter the destructive trajectory will be completely ineffective, and the vehicle could very easily be lost. The difficulties are even more pronounced with an unmanned vehicle, as control in this case rests entirely with the communications network on earth; once re-entry has begun and the plasma sheath has formed the vehicle and its contents are totally committed to one, and only one, re-entry trajectory.

It is believed that a proper solution to the problems of this class (i.e., that class of aerospace vehicle problems which will arise when manned or heavily instrumented extra-terrestrial landers are intended to return to Earth) can be obtained by proper ground testing of aerospace vehicles. To be truly effective such ground testing must be on models of as large a scale as possible. Full scale testing is ideal for many reasons, not the least of which is that actual prototypes can then be studied under actual re-entry conditions. The problem faced in ground testing of aerospace vehicles is quite simply described: one must simulate, at the surface of the test vehicle, the re-entry environment.

The currently popular mechanism selected for this simulation was first publicly described by Brogan[4] who proposed the arc jet as a means of increasing the directed velocity and total enthalpy of air incident on a test object in a "hyperthermal" tunnel. The basic technique[5] has been extended and further developed, until today there are many facilities in the United States devoted almost entirely to the generation and application of high enthalpy hypersonic plasma flows.[6]

The shortcomings of the arc-jet as a gas heater for re-entry simulation were demonstrated by Cann et al[7] who showed that the arc jet is severely limited in enthalpy and efficiency by both radiation losses and contamination of the plasma exhaust by vaporized electrode material. Another approach to the simulation problem has been given by the rotating shock tube design of the Cornell Aeronautical

Laboratories' Wave Superheater.[8] In many respects superior to the arc jet device, the Superheater is, however, unable to simulate an entry trajectory since its maximum operation time is only on the order of 15 seconds and the plasma properties are roughly constant for each operational cycle. Other devices have been suggested, such as the Gerdien Arc,[9] however, they all have been severely limited in application to performance similar to that of the arc jet device: unexpectedly low enthalpy for high power operation with large mass flows, low exhaust velocity, high energy loss through radiation, and contamination of plasma exhaust by electrode and nozzle throat ablation. Unfortunately, neither the previously referenced works, nor any of the recent state-of-the-art surveys[7,10,11] profess much optimism in regard to appreciably increasing the high enthalpy, high power efficiency of the arc jet device; consequently, there is little hope in the forseeable future for true simulation of re-entry conditions if the arc jet is to be employed as the primary gas heater.

On the other hand, recent experimental work with the induced electrodeless discharge has led to what may well be a major breakthrough in the technology of heating air for application in re-entry simulation. Whereas the induced electrodeless discharge has heretofore been generally known as a low power, high frequency curiosity, an easily derived scaling law which greatly extends its capabilities for high power application has not yet been suggested. In the following paragraphs a simple macroscopic theory of the induction field in the electrodeless discharge will be presented, then the physical scaling law will be derived. The scaling law will then be employed to suggest re-entry simulation application for this discharge at extremely high power levels.

Background

The first reported observation of the electrodeless discharge which occurs in a gas within a solenoid carrying high frequency current was made by Hittorf[12] in the latter part of the 19th century. Several minor studies of this curiosity followed, and a semi-complete description of the phenomenon was reported in a classic paper by Sir J. J. Thomson.[13] Assuming the discharge to be magnetic in origin, he later[14] presented his mathematical theory of the discharge which was well supported by experimental proof. J. S. Townsend, who by this time had contributed significantly to the state of knowledge of electrical breakdown in gases, immediately challenged[15] Thomson's work and presented a theory of his own which was equally well supported by experiment. Townsend claimed (and to some extent "proved") that the discharge was electric in nature, while Thomson maintained, and more or less "proved", his stand on the magnetic origin of the induced electrodeless discharge.

The experiments of MacKinnon[16] left little doubt that either mechanism (i.e., the azimuthal electric field resulting from the time rate of change of the axial magnetic induction, or the axial electric field resulting from the potential drop across the solenoid) could, and indeed did excite electrodeless discharges. Later, in the United States, research progressed to the point where it was believed that a conclusive verification of the Thomson theory could be demonstrated. An attempt at verification was made,[17] and some qualitative results were reported,[17,18] however, the technology of this period was most inadequate for the subtility of the measurements which were attempted,[19] and these experiments, for the most part, failed. The difficulty was demonstrated to be the coexistence of the Thomson magnetic discharge and the Townsend electric discharge simultaneously, and in the same apparatus.

The research of the next decade can be summarized by the work of Babat, in whose report[20] is found perhaps the best description ever published of the general properties of electrodeless discharges. It is significant to note that during the period encompassed by Babat's research, Smith[21] was successful in magnetically inducing an electrodeless discharge in Hg vapor with low frequency current supplied by a motor generator.

The thermonuclear age ushered in an era of increasingly better plasma diagnostic techniques. With the advent of Scylla[22] and similar machines, the induced electrodeless discharge became the object of intense study throughout the world, and as a partial result of the new techniques, physical insight, which heretofore had often been lacking, was gained. Carruthers[23] was able to measure the extent of the skin effect and relate it to the electrical conductivity[24] of the plasma in the discharge. Internal magnetic fields were measured.[25] Bolometers for measuring plasma energy losses were developed,[26] and direct measurements of the electrical conductivity of plasmas were reported.[27,28] Meanwhile theory pertinent to the steady state induced discharge advanced. Eckert[29] investigated the breakdown criteria for the ring* discharge and derived the conditions for the transition from free to ambipolar diffusion in this discharge.[30] Hollister[19] extended Thomson's theory of the behavior of the magnetic induction within the induced discharge, and later presented experimental verification thereof.[31,32]

Additional recent experimental advances have pointed the way toward higher efficiencies in electrodeless plasma production. Barger, et al,[33] demonstrated the enhancement in plasma density obtained by the superposition of a low frequency axial magnetic field on the conventional radio frequency discharge. Reed[34] extended the useful operating range of the induced discharge to the high pressure regime, and finally Carswell[35] showed that efficient electrodeless coupling of an electric field to a gaseous discharge is indeed possible, and, in some cases, desirable.

Theory

In general, the electrodeless technique of plasma generation has largely been limited to high frequency operation in what has become known as the "ring" discharge. This discharge is observed when a high frequency axial magnetic field induces azimuthal currents in an ionized gas. The resulting luminosity often appears (along the axis) as a bright ring, hence the name. Electrically the equivalent circuit is given in Figure 1. Physically the transformer is nothing more than a solenoid with a lossy coaxial conductor, in this case a cylinder of ionized gas, as its core.

The impedance of this circuit, as seen by the generator, is given by

$$Z = \left[R_1 + \frac{\omega^2 M^2 R_2}{R_2^2 + \omega^2 L_2^2}\right] + j\omega\left[L_1 - \frac{\omega^2 M^2 L_2}{R_2^2 + \omega^2 L_2^2}\right] . \qquad (1)$$

* The ring discharge is a magnetically induced electrodeless discharge which occurs in the limit of high conductivity, high frequency operation. It is severely skin-effect limited.

If ionization is absent from the secondary its resistance R_2 increases to infinity and no secondary current flows. The impedance of the circuit, as seen by the generator is then given by

$$Z_0 = R_1 + j\omega L_1 \quad . \tag{2}$$

Comparing Eqs. (1) and (2), it is evident that ionization in the coupled circuit increases the overall resistance as seen by the generator, thus for a constant current increasing the losses (i.e., power is transferred to the gas). Also, the inductive reactance of the circuit decreases with coupling to the secondary.

This circuit can be analyzed very efficiently by assuming that in the solenoid configuration the field quantities vary in time as exp ($i\omega t$) and that in the discharge, coaxial with the solenoid, the electrical conductivity can be replaced by a uniform effective conductivity σ. Elimination of the time and electric field from Maxwell's equations then yields an equation for the magnetic flux density $\vec{B}$:

$$\nabla^2\vec{B} - i\sigma\mu_0\omega\vec{B} = 0 \quad . \tag{3}$$

When it is assumed that the magnetic field is entirely axial, as in a long solenoid, and if displacement effects can be ignored (i.e., if $\sigma \gg \omega\epsilon_0$), Eq. (3) is given in cylindrical coordinates by

$$\frac{d^2B_z}{dr^2} + \frac{1}{r}\frac{dB_z}{dr} + i^3\sigma\mu_0\omega B_z = 0 \quad . \tag{4}$$

The solution of Eq. (4) which matches the appropriate boundary conditions (at $r = R$, $B(R) = B_0$; at $r = 0$, $B(0)$ is finite) is:

$$B_z(r) = B_0 \frac{J_0\left(i^{3/2} r\sqrt{\sigma\mu_0\omega}\right)}{J_0\left(i^{3/2} R\sqrt{\sigma\mu_0\omega}\right)} \quad , \tag{5}$$

where the J's are zeroth order Bessel functions with complex argument, r is a distance in the radial direction, and R is the outer boundary of the coaxial plasma.

Noting that in the argument of the Bessel functions

$$r\sqrt{\sigma\mu_0\omega} = \sqrt{2}\, r/\delta \quad ,$$

where $\delta = [2/\sigma\mu_0\omega]^{1/2}$ is the electromagnetic "skin depth" in the plasma, Eq. (5) can be written:

$$B_z(r) = B_0 \frac{J_0\left(\sqrt{2}\, i^{3/2} r/\delta\right)}{J_0\left(\sqrt{2}\, i^{3/2} R/\delta\right)} \quad . \tag{6}$$

At a radius r the current density $\vec{j}$ is given by $(\nabla \times \vec{B})/\mu_o$:

$$\vec{j} = \vec{\phi}\left(-\frac{1}{\mu_o}\frac{\partial B_z}{\partial r}\right). \tag{7}$$

Then

$$j_\phi(r) = i^{3/2}\frac{\sqrt{2}}{\delta\mu_o} B_o \frac{J_1\left(\sqrt{2}\, i^{3/2} r/\delta\right)}{J_o\left(\sqrt{2}\, i^{3/2} R/\delta\right)} \tag{8}$$

is an expression for the radial distribution of the azimuthal current density induced by the magnetic field.

The electric field is given by

$$E_\phi(r) = j_\phi(r)/\sigma = i^{3/2}\frac{\sqrt{2}}{\mu_o\sigma\delta} B_o \frac{J_1\left(\sqrt{2}\, i^{3/2} r/\delta\right)}{J_o\left(\sqrt{2}\, i^{3/4} R/\delta\right)}. \tag{9}$$

The net power transferred into the plasma cylinder per unit surface area is given by the real part of the Poynting vector evaluated at the surface of the cylinder:

$$S = I^2 R/\text{area} = \text{Re}\left[\vec{E}(R) \times \vec{H}^*(R)\right], \tag{10}$$

where RMS values for $\vec{E}$ and $\vec{H}$ have been used.

Equation (10) can be evaluated over the plasma surface to give

$$I^2 R = \frac{2\pi R^3 N^2 \mu_o}{\ell}\omega I^2\left(\frac{\delta}{\sqrt{2}R}\right)\frac{M_1(\sqrt{2}R/\delta)}{M_o(\sqrt{2}R/\delta)}\cos\left[\theta - \theta_o - \pi/4\right] \tag{11}$$

where R is the effective resistance of the plasma cylinder as seen by the generator $\left[= \frac{\omega^2 M^2 R_2}{R_2^2 + \omega^2 L_2^2}\right.$ in Eq. (1)$\left.\right]$ and $B_o = \mu_o NI/\ell$ is the axial field of a long solenoid.

The M's are the moduli of the complex argument Bessel functions and the θ's refer to those functions' phases. I is the rms current in the induction solenoid.

To be thorough, the imaginary part of the Poynting vector can be manipulated to give the inductance of the plasma, as seen by the generator:

$$L_{eff} = \frac{2\pi R^2 N^2 \mu_0}{\ell}\left(\frac{\delta}{\sqrt{2}R}\right)\frac{M_1(\sqrt{2}R/\delta)}{M_0(\sqrt{2}R/\delta)}\sin\left[\theta_1-\theta_0-\pi/4\right],$$

from which the total inductance of the solenoid-plasma transformer is obtained:

$$L = \frac{2\pi R^2 N^2 \mu_0}{\ell}\left(\frac{\delta}{\sqrt{2}R}\right)\frac{M_1(\sqrt{2}R/\delta)}{M_0(\sqrt{2}R/\delta)}\sin\left[\theta_1-\theta_0-\pi/4\right]+\frac{\pi R^2 N^2 \mu_0}{\ell}\left[\frac{A^2}{R^2}-1\right], \quad (12)$$

where A is the radius of the solenoid (A > R).

Experimental verification of Eq. (11) and Eq. (12) has been obtained[19] and reported in the literature.[32]

Equation (11) is of the form

$$(\text{Power/unit vol.}) \sim \left[\omega B_0^2 f(\sqrt{2}R/\delta)\right] \quad (13)$$

where

$$f = 2\frac{\delta}{\sqrt{2}R}\frac{M_1(\sqrt{2}R/\delta)}{M_0(\sqrt{2}R/\delta)}\cos\left[\theta_1(\sqrt{2}R/\delta)-\theta_0(\sqrt{2}R/\delta)-\pi/4\right].$$

When f is plotted against $\sqrt{2}R/\delta$, a maximum is observed in the neighborhood of $\sqrt{2}R/\delta = 2.5$. This is shown in Figure 2, where it can be seen that 2.5 is the value of $\sqrt{2}R/\delta$ for which a maximum amount of power is transferred from the solenoid to the coaxial plasma. In other words, the fact that the coaxial plasma absorbs the most power when $\sqrt{2}R/\delta = 2.5$ can be interpreted as the condition for an impedance match between the primary and secondary of the transformer in Figure 1, hence as the condition for maximum operational efficiency of an induced discharge.

Since $\delta = \left[2/\sigma\mu_0\omega\right]^{1/2}$, this condition can be written

$$R\sqrt{\sigma\mu_0\omega} = 2.5 \quad (14)$$

for maximum efficiency.

One also notes in passing that for uniform energy deposition the assumption of uniform conductivity becomes very good when $R\sqrt{\sigma\mu_0\omega} = 2.5$.

The Scaling Law and Its Application

The ionization per unit volume, hence the electron density n_e, depends on the energy density in the plasma. The energy density is partitioned into thermal, electromagnetic, etc., but ultimately depends on the energy transferred to the plasma from the solenoid. Since the plasma conductivity is proportional to n_e, it follows that the plasma conductivity depends on the plasma energy density. The exact relationship in the induced electrodeless discharge, however, is nonlinear and will be very difficult to formulate. From Eq. (13) however, it appears that an increase in power transfer must be accompanied by an increase in the quantity $\omega B_o^2 f$. Since the internal energy density increases with power the plasma conductivity must also increase. To maintain high efficiency (i.e., an impedance match) the quantity $R\sqrt{\sigma \mu_e \omega}$ must be fixed, so the frequency ω of the magnetic field must be decreased. Therefore, it is qualitatively clear that for a given generator (i.e., solenoid with current flowing) an increase in power must be accompanied by a decrease in frequency, if efficiency in power transfer to the gas is to be maintained.

Likewise it is evident that as the size (i.e., R) of the plasma is increased a corresponding decrease in the quantity $\sqrt{\sigma \mu_e \omega}$ must be effected in order to maintain high efficiency (i.e., $R\sqrt{\sigma \mu_e \omega} = 2.5$). Since σ determines the properties of the discharge and is intended to remain fixed at some high value (on the order of 10^3 - 10^5 mhos per meter in the discharge) to insure a high volume heating rate, the driving frequency of the magnetic field must be decreased to maintain high efficiency as the size of the plasma is increased.

When both the size and the power are increased, it is thus clear that the operating frequency of the field must decrease in order to maintain high efficiency. Hence, it is determined that Eq. (13) and Eq. (14) represent scaling laws for the induced discharge. If sufficient knowledge is obtained for one particular discharge in one particular device it is possible to scale a similar device in size and power to any values desired, so long as operating conditions (i.e., the physics of the situation) don't appreciably change.

At this point one might postulate the existence of an electrodeless discharge apparatus operating in the ultra high power, low frequency regime. By maintaining a flow of high pressure gas (air) into this discharge and expanding the resulting plasma into a vacuum through an appropriate magnetic nozzle, the aerodynamic and thermal conditions of re-entry may be simulated in a downstream test section.[32] If the theoretical scaling laws previously stated can be shown to hold, a full scale re-entry simulator could be designed and constructed. Rather than operate on a conventional V-I characteristic curve as does the arc, the induced discharge, being a volume phenomenon, changes its physical size and internal distributions in field intensity and species' densities with changing field parameters (i.e., B, J, ω). Thus, it is expected that the electrodeless discharge can be maintained over widely varying conditions of gas density, mass flow, and applied power. When it is shown that this is indeed the case it will be possible to design a facility for re-entry ground testing that will closely reproduce the conditions of the entire re-entry trajectory at the surface of a test object. The scaling laws will then permit the extension of this concept to the full scale case. Through proper manipulation of the controlling networks for regulating mass flow to the discharge, power to the discharge, the frequency of the power and current to the magnetic nozzle, close duplication of the conditions of the re-entry trajectory will obtain. Since it is an easy matter to machine-control such parameters as gas flow, power, driving frequency, and current, it appears feasible to reduce the simulated test trajectory to data on a stack of computer cards, and, with sufficient feedback data from sensors in the test object, let the entire operation be computer-controlled.

Thus the design for a pre-programmed full scale re-entry simulator, capable of reproducing the conditions of an arbitrary trajectory in an arbitrary atmosphere at the surface of a test object can be effected. Such a concept is impossible with the arc jet in today's technology.

Optimization of the Electrodeless Discharge

In order to fully appreciate the advantages offered by the magnetically induced electrodeless discharge, one must compare its performance with that of a conventional arc, or some similar heater, at conditions of similar power, enthalpy, or temperature. The basic energy loss mechanisms for the arc discharge were treated by Cann, et al.[7,10] In these reports it is concluded that for very small discharge chambers and low pressure operation the major wall loss mechanism is combined in convection and conduction. In the case of large discharge chambers and high pressures the radiant heat flux dominates. It is possible, however, that for large chamber sizes (relative to the size of a typical arc chamber) and at very high power levels, a mechanism exists to trap much of the radiant energy in the plasma so that much higher mean enthalpies become possible. One cannot, however, hope to totally eliminate the radiation problem. In general, a system in thermodynamic equilibrium at a temperature T radiates energy from its surface at a rate proportional to T^4. It is therefore clear that temperature radiation losses are an important problem in high temperature plasma systems, and that such losses increase rapidly with temperature. One might hope, however, to minimize the extent of this loss mechanism by generating a physically large discharge under such conditions as to produce an optically dense[36,38] plasma in the frequency interval of maximum radiation intensity.

The mean free path for optical radiation in air, derived[37] from the Rosseland mean absorption coefficient, is given as a function of air temperature (1 volt = 11,600°K) for various gas densities in Figure 3. In this figure it is shown that the opacity of an air plasma increases with density, and at temperatures on the order of two volts, for relative densities greater than unity ($\frac{\rho}{\rho_o} = 1.2931 \times 10^{-3}$ gm/cm^3) the mean free path for radiation is on the order of millimeters. Thus it is expected that considerable self-absorption of the core radiation will occur in nearby gaseous layers in such a physically large hot discharge. These outer layers, in turn, radiate into still cooler layers of gas, but again, the mean free path for radiation is short, and this radiation also is absorbed, and so on. The net effect is a tendency toward the flattening of the discharge temperature profile through the raising of the temperature of the outer plasma layers, and a surface radiation loss characteristic of a temperature much less than the "average" temperature of the gas (i.e., the discharge efficiency is raised), because of the inability of the radiation to escape from the hot plasma volume.

Radiation, however, is not the entire problem. The arc jet, when operated at high levels of power, can usually be characterized by power densities on the order of several megawatts per square centimeter of electrode surface, yielding severe evaporation of electrode material during operation, and consequently, short electrode operation times. Additionally, contamination of the exhaust plasma by electrode material further limits the usefulness of the conventional arc jet device in re-entry simulation applications. Thus, in addition to wall losses (including conductive and convective nozzle losses) electrode losses must also be considered in the evaluation of a plasma device in the re-entry simulation application. Since there are no electrodes in the induced discharge, this problem is bypassed.

The conductive and convective heat transfer mechanisms at the wall can be reduced by noting that in the electrodeless discharge most of the conductive and convective energy transported to the wall is transported by ionized particles. Such carriers experience a retarding (i.e., Lorentz) force when they cross a magnetic field, hence the installation of a very strong magnetic field at the wall, parallel to the axis of the discharge, will partially confine the plasma in the resulting "magnetic cylinder". Such a magnetic field is produced by a short solenoid, and has the advantage that the magnetic flux density, hence the particle confinement, is strongest near the solenoid, hence near the wall of the discharge chamber in the cylindrical geometry. An additional inward directed body force ($\vec{J}_\phi \times \vec{B}_z$) greatly enhances the magnetic bottle effect in the high power (e.g., high current) induced discharge to further reduce the wall heat transfer by conduction and convection.

The final magnitude of the plasma jet velocity will be largely determined by the effective area of the sonic throat of a deLaval nozzle exhausting into an evacuated test chamber. Since the exhaust velocity and mass flow vary continuously during the simulated trajectory, the effective throat area and pressure drop across the throat must be continuously varied. The extreme temperatures and large mass flow rates which exist at the throat preclude the use of any mechanically adjustable device, hence require the utilization of an efficient magnetic system.[39]

The magnetic nozzle is of the "hybrid" variety; that is, it is a conventional sonic orfice with a steady superimposed magnetic field as in Figure 4. The magnitude of the field is then adjusted to artificially regulate the effective size of the orfice through the application of a magnetic pressure on the ionized gas.

It is assumed that the particles passing through this hybrid orfice are electrons or singly ionized atoms in equilibrium at an initial temperature T. Each such particle then experiences a force F at the nozzle.

$$\vec{F} = m\dot{\vec{v}} = e\left(\vec{v} \times \vec{B}\right) , \tag{15}$$

from which is derived the equation of motion for the particle in the axial direction

$$m\dot{v}_z = e\, v_\phi\, B_r , \tag{16}$$

where the particle has been assumed to have a mass m, a charge e, and the azimuthal component of the magnetic field has been taken as zero.

Since $\nabla\cdot\vec{B} = \frac{1}{r}\frac{\partial}{\partial r}(rB_r) + \frac{1}{r}\frac{\partial B_\phi}{\partial \phi} + \frac{\partial B_z}{\partial z} = 0$ and $B_\phi = 0$, one can obtain

$$\frac{\partial}{\partial r}(rB_r) = -r\frac{\partial B_z}{\partial z} . \tag{17}$$

The radius of gyration ρ of the particle in the field B is given by

$$\rho = \frac{m v_\perp}{e B} \ll L \quad ,$$

where L is the physical diameter of the throat. If $(\partial/\partial z) B_z$ can be considered independent of r, Eq. (17) can be directly integrated to yield

$$B_r = -\frac{r}{2} \frac{dB_z}{dz} \quad . \tag{18}$$

Eq. (18) can be evaluated at $r = \rho$ to give

$$B_r\Big|_{r=\rho} = -\frac{\rho}{2} \frac{dB_z}{dz} \quad . \tag{19}$$

Substituting Eq. (19) into Eq. (16) gives

$$m \dot{v}_\parallel = -e \frac{v_\perp \rho}{2} \frac{dB_z}{dz} \quad , \tag{20}$$

where $v_\perp = v_\phi$ denotes motion perpendicular to the field B, and $\dot{v}_\parallel = \dot{v}_z$ denotes acceleration parallel to the field.

The magnetic moment μ of the gyrating particle is given by

$$\mu = \frac{1/2\, m v_\perp^2}{B} = \frac{1}{2} e v_\perp \rho \quad , \tag{21}$$

and is invariant in a cylindrically symmetric magnetic field.[40]

Inserting Eq. (21) in Eq. (20) yields

$$m \dot{v}_\parallel = -\mu \frac{dB_z}{dz} = F_\parallel \quad . \tag{22}$$

Equation (22) suggests that the force $F_\parallel$ is directed opposite the particle's motion and is proportional to the axial gradient of the field. Since the magnetic moment μ is positive for particles of both signs of charge, it is clear the $F_\parallel$ is always directed against the field direction for the converging field existing at the entrance to the magnetic nozzle. On the exit side the field diverges making

$(1/dz)B_z<0$, hence the force F_R in this region accelerates charged particles away from the nozzle. The effective size of the nozzle is determined by the magnitude of the force F_R, hence, for a constant magnet geometry, to increase the effective size of the throat the magnitude of the magnetic field is decreased; to decrease the effective size of the throat the magnitude of the magnetic field is increased.

On the other side of the coin, one must realize that there is no panacea for the ills of high temperature physics. Such an elixir has always been the result of careful research, and so it is here. There are still problems associated with arc-jet (and other) plasma devices which are common with the induced electrodeless discharge. Gas still radiates as T^4 and materials (even high temperature insulators) still melt and ablate. Ways and means for further minimizing or eliminating these difficulties must yet be found.

A difficulty unique with the induced discharge arises from the time varying nature of the induction field. This is demonstrated by integrating the equation of continuity for electrons

$$\frac{dn_e}{dt} = (\nu_i - \nu_a) n_e + \nabla^2 (D n_e) \quad , \tag{23}$$

where n_e is the electron density, ν_i is the ionization rate, ν_a is the de-ionization rate and D is the diffusion rate. The diffusion term can be neglected in the high pressure electrodeless discharge because in a characteristic relaxation time τ, $L' > \sqrt{D\tau}$, where L' is a characteristic dimension of the discharge chamber. The integral of (23), evaluated at the characteristic time τ is then given by

$$n(\tau) = n_o \exp(\nu_i - \nu_a)\tau \quad , \tag{24}$$

where $n(\tau)$ is the electron density after a time τ and n_o is the initial electron density. Solution of equation (24) for the relaxation time τ then yields

$$\tau = \frac{1}{\nu_i - \nu_a} \log_e \frac{n(\tau)}{n_o} \quad . \tag{25}$$

For the discharge to continue between half cycle crests of the exciting field, it must be true that $\tau > \frac{1}{2}T$, where T is the period of the field. This places a lower limit on the operation frequency of the field for all cases where auxiliary ionization is not employed. This frequency is given by

$$f > \frac{\nu_i - \nu_a}{2 \log_e \frac{n(\tau)}{n_o}} \quad . \tag{26}$$

Since the fractional reduction in electron number density $n(\tau)/n_o$ appears in Eq. (26) only logarithmically, it is seen that the lower limit frequency depends much more strongly on the electron production rate than it does on the electron number density. When the induction field swings through zero amplitude its

contribution to ν_i vanishes, leaving only the thermal contributions to ν_i from photoionization (i.e., self-absorption) and electron impact. Depending on the dominant de-ionization process ν_i may then become negligible in comparison with ν_a and the frequency necessary to maintain the discharge will rise to a very high value. This would clearly defeat the purpose of the scaling law. For three-body recombination in air at pressures in excess of about ten atmospheres this rate is roughly 10^7 sec^{-1}. Ignoring any contribution to ν_i by photoionization, the relaxation time τ for a fractional electron density between 10^{-3} and 10^{-6} is then between 10^{-5} and 10^{-6} seconds. If this time interval is considered to represent a maximum of 10% of the induction half cycle, it becomes apparent that a lower limit indeed exists for the frequency of the electromagnetic radiation driving the discharge. The data presented above yield a lower limit in frequency of 5 to 50 kc/sec, but from the approximate nature of this analysis this figure can only represent the order of magnitude for the lower limit.

In the case of dissociative recombination which would occur at low temperatures in high pressure air, the de-ionization rate could be several orders of magnitude larger than it was in the three body case. Fortunately, in this case, auxiliary ionization with high frequency power between crests of the low frequency discharge is both compatible with the scaling law and suitable for the maintenance of the discharge between cycles. The effect of such auxiliary ionization on Eq. (26) is to increase the magnitude of ν_i, thus yielding a reduced value for the lower limit discharge frequency.

A Full Scale Re-entry Simulator

The conditions for "true" re-entry simulation were recently stated by Cann et al.[7] The following time varying quantities in the simulation facility must be the same as their time varying free flight values:

1. Gas composition (atmospheric air).
2. Total enthalpy.
3. Mach number (i.e., gas velocity).
4. One of the following:
   a. Reynolds number based on model size.
   b. Model surface pressure (or R_e per unit length)
   c. Surface heat transfer rate, $\dot{q}$.
5. Run durations of the same order of magnitude as the re-entry maneuver being simulated (i.e., continuous operation).

Conditions 1 and 5 are not difficult to achieve with the electrodeless discharge technique. In the high power, high pressure electrodeless discharge the plasma will be both physically large and optically thick, hence considerable self-absorption of radiation will result in a higher internal temperature than that characteristic of the surface radiation loss. A much higher mean enthalpy will therefore obtain in the electrodeless discharge than in the arc device for a given power input. By a proper matching of the discharge enthalpy with the exhaust enthalpy through the magnetic throat it appears that items 2 and 3 may be closely approximated, if not exactly duplicated in the downstream test section.

Simulation of the Reynolds number will clearly be less difficult in the full scale case than in the case of a small model, although the total effect of residual ionization and dissociation in the exhaust jet on the density and viscosity of the

Table I

Facility Design Parameters for Simulation of Prescribed Superorbital Re-entry Trajectory

Time (sec)	Velocity (ft/sec)	Altitude (ft)	H/RT_o	P_T (atm)	$T(^oK)$	P_{exit} (torr)	M	A/A*	D* (cm)	$\dot{w}$(lb/sec)	Power (Kw)
0	3.6×10^4	4×10^5	775	-	-	-	-	-	-	-	-
100	3.45×10^4	2.3×10^5	721	-	-	-	-	-	-	-	-
200	3×10^4	2.36×10^5	531	-	-	-	-	-	-	-	-
300	2.82×10^4	2.48×10^5	470	725	11,700	4×10^{-6}	26.8	3.55×10^8	0.016	9.3×10^{-4}	15.5
400	2.68×10^4	2.56×10^5	431	652	11,200	2.2×10^{-6}	27.7	5.39×10^8	0.0132	5.7×10^{-4}	8.76
500	2.58×10^4	2.59×10^5	396	603	10,800	1.36×10^{-6}	28.6	7.13×10^8	0.0115	4.08×10^{-4}	5.75
600	2.52×10^4	2.59×10^5	372	576	10,500	1.3×10^{-6}	28.6	7.13×10^8	0.0114	4.08×10^{-4}	5.42
700	2.46×10^4	2.59×10^5	359	556	10,300	1.25×10^{-6}	28.6	7.13×10^8	0.0114	3.97×10^{-4}	5.07
800	2.39×10^4	2.58×10^5	340	532	10,100	1.28×10^{-6}	28.5	7×10^8	0.012	3.96×10^{-4}	4.8
900	2.29×10^4	2.48×10^5	312	502	9,700	2.79×10^{-6}	26.6	3.5×10^8	0.016	7.85×10^{-4}	8.6
1000	2.15×10^4	2.3×10^5	272	453	9,150	6.22×10^{-6}	24.6	1.6×10^8	0.024	1.56×10^{-3}	15.15
1100	1.93×10^4	2.18×10^5	219	381	8,300	2×10^{-5}	21.6	4.6×10^7	0.045	5.1×10^{-3}	39.8
1200	1.62×10^4	2×10^5	153	288	6,700	7.42×10^{-5}	19.2	1.47×10^7	0.080	1.39×10^{-2}	75.6
1300	1.19×10^4	1.72×10^5	85	170	4,500	4.79×10^{-4}	15.6	2×10^6	0.215	7.75×10^{-2}	237
1400	6.9×10^3	1.42×10^5	29	72.5	2,000	1.54×10^{-3}	13.1	3.82×10^5	0.494	2.78×10^{-1}	287
1500	2.6×10^3	9.8×10^4	4.6	-	-	-	-	-	-	-	-

Conditions: P/P_o = 10 in discharge; D_{exit} = 10 feet

gas near the model is yet to be determined. In the full scale case, then, condition 4 will be approximately fulfilled.

As an example of the range in parameters of a re-entry trajectory that might be simulated, consider the hypothetical re-entry trajectory presented in Figure 5 where the velocity and altitude of a re-entering superorbital vehicle in a "skip" trajectory are given as functions of time. Data have been obtained for the design of apparatus for the simulation of the major portion of this trajectory and are presented in Table I. Although the design characteristics of a facility to duplicate this trajectory are severe, such a facility is not beyond the present state of the art, provided, of course, that the electrodeless discharge and magnetic nozzle are employed in this facility.

Future Research

The power requirements, physical size and total cost of a full scale re-entry simulator are such as to demand a very careful laboratory evaluation of the concept preliminary to undertaking the final design. A model simulator is therefore to be constructed and its plasma properties and operating characteristics carefully measured and compared with theory.

The primary goal of this preliminary study is the experimental verification of the physical scaling laws, and the determination of the limits of applicability for these laws, if such limits exist. A secondary goal is the development of a suitable magnetic nozzle for the expansion of hot plasmas to high Mach numbers. The experimental program will consist mainly of a thorough measurement of the hypersonic aerodynamic flow parameters and their comparison with typical arc-jet values, and simultaneous detailed physical measurements of the plasma discharge itself.

The discharge is to be energized by means of MOPA apparatus (i.e., Master Oscillator, Power Amplifier). This permits the variation of applied frequency over the design range of the electronics system (about two decades from 50 kc/sec to 5 Mc/sec) so that all measurements of the discharge parameters can be made as functions of frequency as well as power. The power output of this apparatus is fifty kilowatts over the design frequency range. A block diagram of the experimental device is presented in Figure 6.

The discharge tube is made of a high temperature dielectric material (Boron Nitride or Alumina). For the initial measurements a two inch diameter discharge tube is used; later in the program the diameter of the discharge tube can be varied (1", 3", 4") in order to experimentally demonstrate the relationship between discharge radius and applied frequency, for cases of equal energy density (i.e., similar plasmas).

Within the discharge the spatial distribution in electron number density n_e must be carefully determined as a function of frequency, power and initial gas pressure. Clearly, in the pressure and enthalpy regime of conditions existing in the high power electrodeless discharge, conventional electron density measuring techniques (i.e., the Langmuir probe, the microwave interferometer) cannot be employed. The Langmuir probe[41] is ineffective at high pressures because its physical size, which must be smaller than the ion or electron mean free path in the plasma, necessarily becomes very small and the probe becomes extremely susceptible to rapid and uncontrollable heating, yielding thermal emission of electrons from its surface and resulting in meaningless probe data. The microwave interferometer[42,43,44] is

employed in plasma diagnostics at a frequency greater than the "plasma" (or "cutoff") frequency ν_p. Numerically this frequency is given by

$$\nu_p = 8.98(n_e)^{1/2} \quad \text{kc/sec} \quad ,$$

where n_e is the electron number density (cm^{-3}). With presently available microwave generators the upper limit in measurable electron concentrations is therefore seen to be on the order of 10^{14} cm^{-3}, a value less than that anticipated for the high pressure electrodeless discharge.

An optical technique has recently been developed however, which removes the frequency restriction characteristic of microwave procedures yet retains the advantage of requiring no material contact with the plasma.[45-49] Specifically, reference is made to the infrared laser interferometer.

The index of refraction χ of a plasma for electromagnetic radiation at angular frequency ω is

$$\chi = 1 - \tfrac{1}{2}(\omega_p/\omega)^2 \quad , \tag{27}$$

where the plasma radian frequency ω_p in MKSQ units is

$$\omega_p^2 = (2\pi\nu_p)^2 = n_e e^2/m_e\epsilon_0 \quad , \tag{28}$$

and it is assumed that $\omega^2 \gg \omega_p^2$. Thus, as in the microwave case, the index of refraction of a plasma can be measured with an interferometer to determine the plasma free electron density.

The number N of interference fringes produced by a plasma of length $\tilde{L}$ is given by

$$N = (\chi - 1)\frac{\tilde{L}}{\lambda} \tag{29}$$

where λ is the wavelength of the radiation. In the technique of Ashby and Jephcott[49] the laser output through the plasma is reflected back on itself through the plasma, and back into the laser as in Figure 7. The path length is now $2\tilde{L}$ and the total number of fringes observed is

$$N = \left(\frac{\omega_p}{\omega}\right)^2 \frac{\tilde{L}}{\lambda}$$

$$\therefore \quad N \simeq 8.9 \times 10^{-16}\, n_e \tilde{L} \lambda \; ;$$

Hence,

$$n_e = \frac{N}{8.9\,\ell\lambda} \times 10^{16} \text{ per meter}^3,$$

$$n_e = 3.3 \times 10^{20}\, N/\ell \qquad (\lambda = 3.391\mu, \text{ IR})$$

From a consideration of the limiting plasma frequency it is determined that in the case of a He - Ne laser (output radiation at $\lambda = 3.391\mu$ - infrared, and at $\lambda = 0.6328\mu$ - visible) this technique can be applied to the diagnostics of cases where the electron number density approaches 10^{20} cm^{-3}.

The electron number density distribution can thus be determined as a function of discharge current frequency, power, and initial gas pressure, by a simple radial survey of the electron number density measured in the axial direction.

Part of the incident laser radiation will be scattered out of the plasma by free plasma electrons (Thomson scattering). The frequency spectrum of this radiation will be Doppler broadened to an extent determined by the square root of the electron temperature. One therefore measures the spectral distribution of this radiation to determine the electron temperature in the discharge, as a function of discharge current frequency, power, and initial gas pressure. By making these measurements simultaneous with the electron density distribution measurements the radial distribution in electron temperature is obtained.

Knowledge of the electron density and temperature, and the initial gas composition (air) and pressure permits the compution of the electrical conductivity in the discharge. In this exercise the conductivity distribution $\sigma(r)$ is obtained as a function of discharge current frequency, power, and initial gas pressure.

In Eq. (11) the power transferred to the gas was given by

$$I^2R = \frac{2\pi R^2 N^4 \mu_0}{\ell}\,\omega\, I^2 \left(\frac{\delta}{\sqrt{2}R}\right) \frac{M_1(\sqrt{2}R/\delta)}{M_0(\sqrt{2}R/\delta)} \cos\left[\theta_1 - \theta_0 - \pi/4\right], \qquad (11')$$

where I is the rms current in the induction solenoid. The left hand side of this expression is directly measured with an in-line wattmeter, and the frequency and rms current are measured by standard techniques. The equation is then solved for the quantity

$$2\left(\frac{\delta}{\sqrt{2}R}\right) \frac{M_1(\sqrt{2}R/\delta)}{M_0(\sqrt{2}R/\delta)} \cos\left[\theta_1 - \theta_0 - \pi/4\right]$$

which determines $R\sqrt{\sigma\mu_0\omega} = \sqrt{2}R/\delta$. Assuming the conductivity to be roughly constant its effective value can be determined.

In the pressure-temperature-frequency regime of interest the electrical conductivity is given by

$$\sigma = \frac{n_e e^2}{m_e \nu_c}$$

where ν_c is the frequency of elastic electron-neutral collisions.* For a given set of discharge conditions the electron number density n_e is measured as a function of radius with the laser interferometer. The actual radial distribution of conductivity $\sigma(r)$ is then formed as a function of power, pressure and frequency, and is then compared with the effective value obtained from the power measurement at the same discharge conditions. The effect on the impedance of the plasma cylinder of a nonuniform distribution in electrical conductivity can then be determined. From this information several discharge devices of varying diameter are to be designed and constructed. Measurements of n_e, σ, and power will then be made in the neighborhood of $\sqrt{2}R/\delta = 2.5$. Final verification of the scaling law will result from these measurements.

The measurements to be made in the expanded jet are those of static and total pressure, total enthalpy, local mass flow and velocity. These data, obtained by applying standard arc-jet diagnostic procedures are compared to published arc-jet operating specifications[6] to determine the relative efficiency of the induced discharge as a gas heater.

A technique recently described[28] for direct conductivity measurements will be employed to determine the electrical state of the plasma jet. The jet is situated within the volume of a solenoid, or equivalent field generating device, which carries a weak rf current. Eddy currents are induced in the conducting jet according to Faraday's law of induction, and the resultant decrease in magnetic flux in the jet volume is experimentally observed. This quantity is then related to the plasma conductivity through the skin depth relation. The apparatus to be used in this diagnosis is depicted in Figure 8. With this apparatus a spatial-temporal history of the plasma jet conductivity is obtained on the recorded output of a multi-channel strip chart recorder, and can be displayed as a function of applied power, frequency, enthalpy, etc., in order to aid jet optimization studies.

Acknowledgement

The author is especially thankful to Stanley R. Byron for both his critical evaluation of the manuscript and for our many stimulating discussions during its preparation. Special acknowledgement is also due Robert E. Price, who performed most of the aerodynamic calculations.

---

* Values of ν_c for various gases and gas mixtures are given by Sanborn Brown as a function of electron energy and density in "Basic Data of Plasma Physics", MIT Press 1961.

References

1. Leonard Roberts, "Entry into Planetary Atmospheres," Astronautics and Aeronautics, Vol. 2, No. 10, pp 22-29, October 1964.
2. Lyman Spitzer, "Physics of Fully Ionized Gases," Interscience Publishers, Inc., 1956, p 50, equations 4-7.
3. G. P. Kuiper, editor, "The Sun," University of Chicago Press, 1953, pp 469-474.
4. Thomas R. Brogan, "Electric Arc Gas Heaters for Re-entry Simulation and Space Propulsion," ARS preprint number 724-58, November 1958.
5. Finkelnburg, W. and Maecker, H., Handbuch der Physik, Vol. 22, Springer-Berlin, 1956.
6. An impressive survey of the capabilities of presently existing plasma jet devices was recently prepared by D. J. Tillian: "Plasma Arc Facilities in the United States," Report number 0-71000/3R-22, November 1963, Ling, Temco, Vought Research Center, P. O. Box 5003, Dallas, Texas.
7. G. L. Cann, et al, "Magnetogasdynamic Accelerator Techniques," Report AEDC-TDR-62-145, July 1962, ASTIA Document Number 277954.
8. "Wave Superheater Hypersonic Tunnel," Cornell Aeronautical Laboratory, October 1960.
9. Helmut E. Weber and John H. McGinn, "A Constricted Arc for High Energy Gas Flow," Aerospace Engineering, 22, 202 (1963).
10. G. L. Cann, R. D. Buhler, R. L. Harder, R. A. Moore, "Basic Research on Gas Flows through Electric Arcs - Hot Gas Containment Limits," ARL Report 64-49, March 1964.
11. Julio Cordero, Franklin W. Diederich, Henryk Hurwicz, "Aerothermodynamic Test Techniques for Re-entry Structures and Materials," Aerospace Engineering, 22, 166 (1963).
12. W. Hittorf, Ann. Physik, 21, 137 (1884).
13. Thomson, J. J., Phil. Mag., (S.5), 32, 321 (1891); (S.5), 32, 445 (1891).
14. Thomson, J. J., Phil. Mag. (S.7) 4, 1128 (1927)
15. Townsend, J. S. and Donaldson, R. H., Phil. Mag. (S.7) 5, 178 (1928)
16. MacKinnon, K. A., Phil. Mag. (8) 605 (1929).
17. Tykocinski-Tykociner, J., Phil. Mag. 13, 953 (1932).
18. Kunz, J., Phil. Mag. 13, 964 (1932).
19. Hollister, D. D., Bull. Amer. Phys. Soc. 7, 441 (1962).
20. Babat, G., J. Inst. Elect. Engr. (London) 94, 27 (1947).
21. Smith, C. G., Phys. Rev. 59, 997 (1941).
22. See, for example: Elmore, W. C., et al, Paper 15/P/356, Second U. N. International Conf. on the Peaceful Uses of Atomic Energy, Geneva, 1958;
    Kvartskhava, I. F., et al, Soviet Physics-Technical Physics 5, 1253 (1961);
    Andryuk, E. D., et al, Soviet Physics-Technical Physics 5, 497 (1960).
23. Carruthers, R., Appl. Sci. Res. 5, 135 (1955).
24. Mohler, F. L., Jour. Res. Nat'l Bur. Std. 21, 873 (1938).
25. Jahoda, F. C. and Sawyer, G. A., Phys. Fluids 6, 1195 (1963).
26. Gorelik, L. L. and Sinitsyn, V. V., Soviet Physics - Technical Physics 9, 393 (1964).
27. Olson, R. A. and Lary, E. C., Rev. Sci. Instr. 33, 1350 (1962).
28. Hollister, D. D., Bull. Amer. Phys. Soc. 7, 373 (1962), also AIAA Jour. 2, 1568 (1964).
29. Eckert, H. U., Bull. Amer. Phys. Soc. 5, 371 (1960).
30. Eckert H. U., Jour. Appl. Phys. 33, 2780 (1962).

31. Francis, G., Ionization Phenomena in Gases, Academic Press, Inc., New York 1960, p 137.
32. Hollister, D. D., IEEE Trans. PTGAP, AP 13, 134 (1965).
33. Barger, R. L., Brooks, J. D., and Beasley, W. D., NASA TN D-1004, Feb. 1962.
34. Reed, T. B., Jour. Appl. Phys. 32, 821 (1961).
35. Carswell, A. I., Rev. Sci. Instr. 34, 1015 (1963).
36. S. Chandrasekhar, Radiative Transfer, Dover Publication, Inc., New York 1950, Chapter 1.
37. Armstrong, B. H., et al, J. Quant. Spectrosc. Radiat. Transfer. 1, 143 (1961).
38. Lawrence H., Aller, "Astrophysics, The Atmospheres of the Sun and Stars," Ronald Press Company, New York, 1963, pp 101-106.
39. Donald J. Spencer, Rev. Sci. Instr. 35, 409 (1964).
40. David J. Rose and Melville Clark, "Plasmas and Controlled Fusion," Wiley and Sons, Inc., New York, 1961, pp 209-213.
41. Langmuir, I., and Mott Smith H. M., Gen. Elec. Rev. 26, 731 (1923); 27, 449 (1924); 27, 583 (1924); 27, 616 (1924); 27, 726 (1924); 27, 810 (1924); see also Gourdine, M. C., and Hollister, D. D., PLR-105 Plasmadyne Corp., Santa Ana, Calif., 15 Sept. 1961; also reference 32.
42. Warton, C. B., and Slager, D. M., IRE Transactions PGNS 6, 20 (1959).
43. Jahn, R. G., Phys. Fluids, 5, 678 (1962).
44. Talbot, L., Katz, J. E., and Brundin, C. L., Phys. Fluids 6, 559 (1963).
45. D.E.T.F Ashby, Appl. Phys. Letters, 3, 13 (1963).
46. J. B. Gerardo and J. T. Verdeyen, Appl. Phys. Letters, 3, 121 (1963).
47. R. F. Gribble, J. P. Craig, and A. A. Dougal, Appl. Phys. Letters, 6, 50 (1964).
38. A. Gibson and G. W. Reid, Appl. Phys. Letters, 5, 195 (1964).
49. D.E.T.F. Ashby, et al, J. Appl. Phys. 36, 29 (1965).

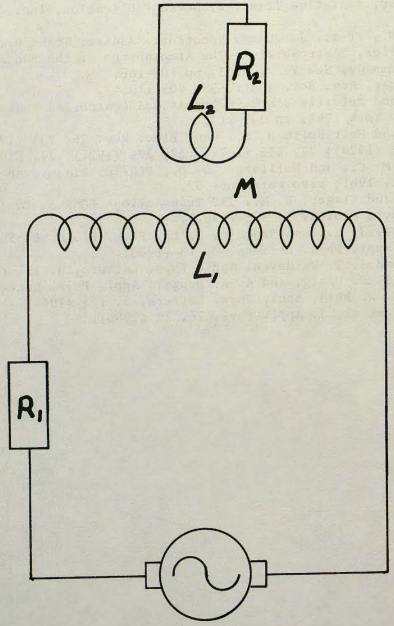

Figure 1. Equivalent Circuit of Plasma Generator

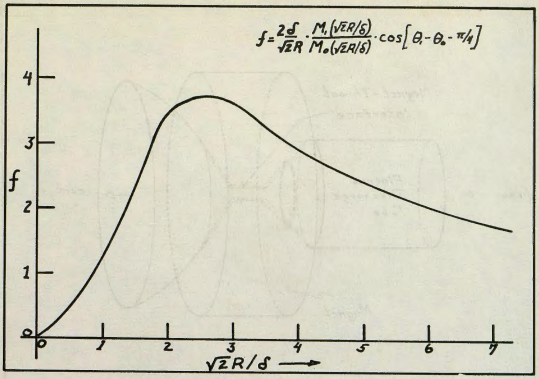

Figure 2. $f(\sqrt{2}R/\delta)$ as a Function of $2R/$

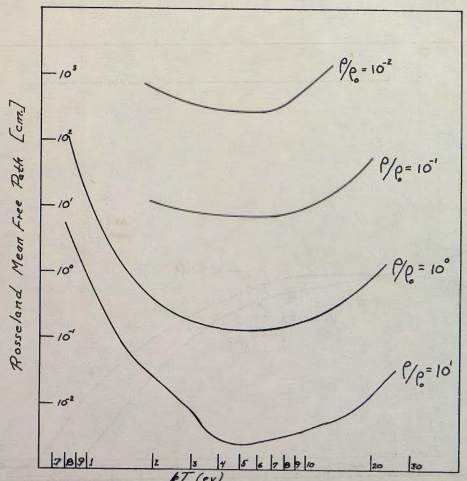

Figure 3. Rosseland Mean Free Path in Air as a Function of Temperature

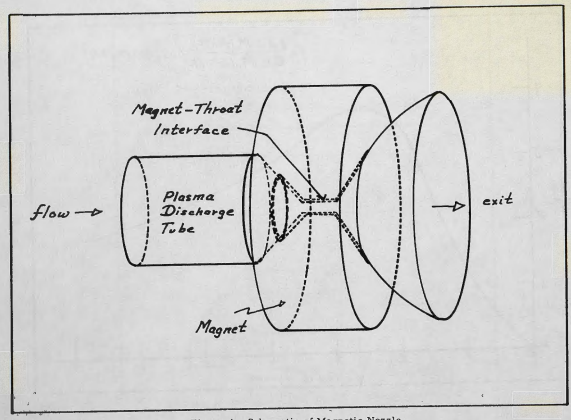

Figure 4. Schematic of Magnetic Nozzle

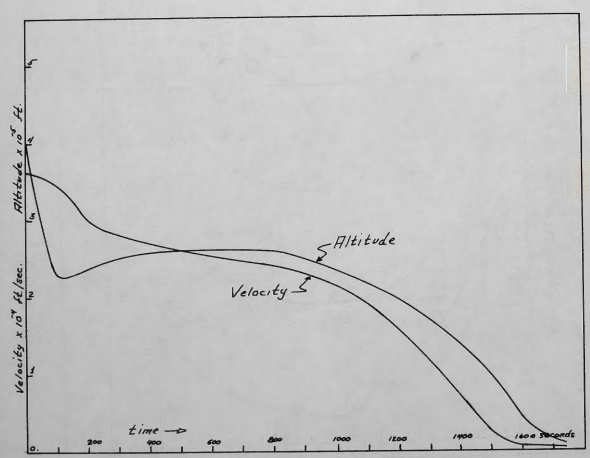

Figure 5. An Earth Entry Trajectory for Superorbital Velocities

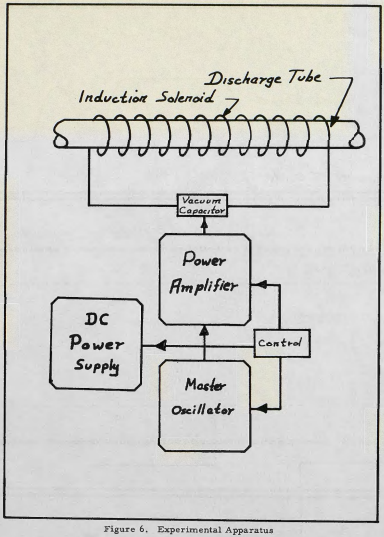

Figure 6. Experimental Apparatus

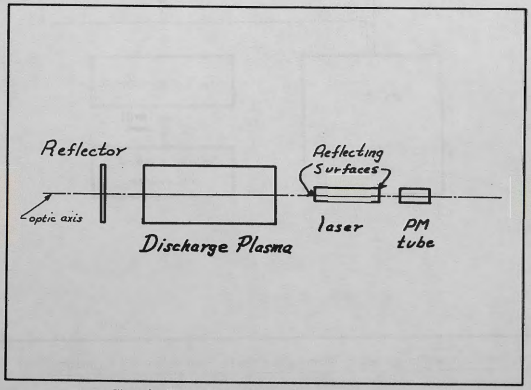

Figure 7. Plasma Diagnostic Measurement: Electron Density

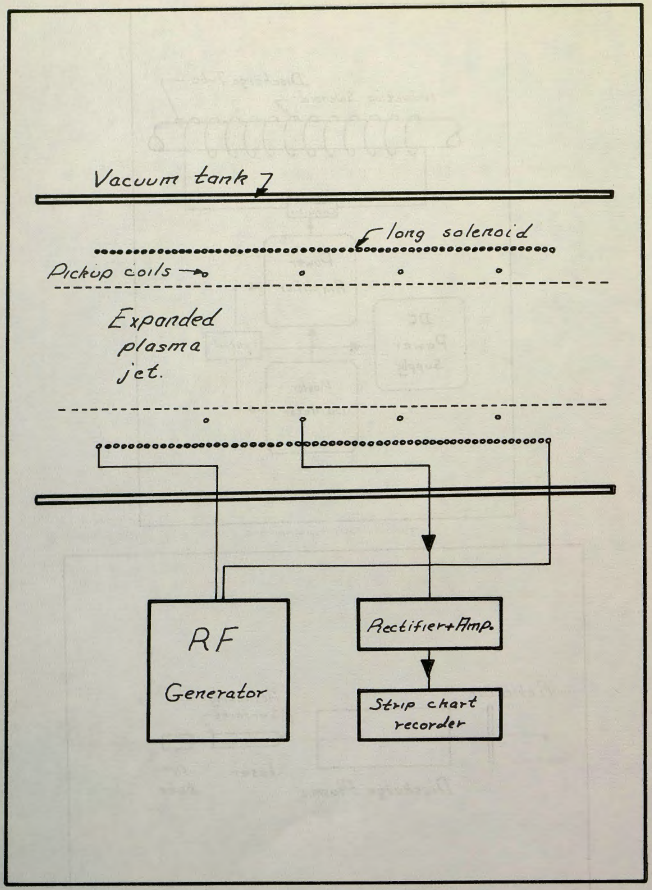

Figure 8. Plasma Diagnostic Measurement: Electrical Conductivity of Jet